The following Communications have been judged by at least two referees to be "very important papers" and will be published online at www.angewandte.org soon:

*I. Garcia-Bosch, A. Company, C. W. Cady, S. Styring, W. R. Browne, X. Ribas, M. Costas**
Evidence for a Precursor Complex in C–H Hydrogen-Atom-Transfer Reactions Mediated by a Manganese(IV) Oxo Complex

*G. N. Newton, S. Yamashita, K. Hasumi, J. Matsuno, N. Yoshida, M. Nihei, T. Shiga, M. Nakano, H. Nojiri, W. Wernsdorfer, H. Oshio**
Redox-Controlled Optimization of the Magnetic Properties of Keggin-Type $\{Mn_{13}\}$ Clusters

J. J. Murphy, A. Quintard, P. McArdle, A. Alexakis, J. C. Stephens**
Asymmetric Organocatalytic 1,6-Conjugate Addition of Aldehydes to Dienic Sulfones

*S. Zhou, S. Fleischer, K. Junge, M. Beller**
Cooperative Transition-Metal and Chiral Brønsted Acid Catalysis: Enantioselective Hydrogenation of Imines to Amines

*J. M Lee, W. Shim, J.-S. Noh, W. Lee**
Highly Mobile Thin Films on an Elastomeric Substrate as Gas Sensors: Palladium-Based Nanogap Hydrogen-Gas Sensors

Author Profile

*"My favorite food is Spanish ham.
The most significant scientific advance of the last hundred years has been the discovery of the laser ..."*
This and more about José L. Alonso can be found on page 5422.

News


J. W. Bode


D. Crich


R. H. Grubbs


C. J. Hawker


D. W. C. MacMillan


K. Maruoka


K. Matyjaszewski


K. Müllen


R. R. Schmidt


V. V. Zhdankin

Books

Contents

Highlights

Surface Modification

R. Manova, T. A. van Beek,
H. Zuilhof* ______________ **5428 – 5430**

Surface Functionalization by Strain-Promoted Alkyne–Azide Click Reactions

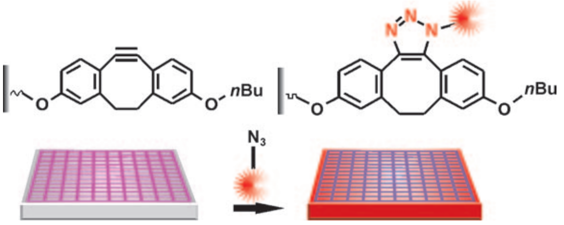

Clicks without Cu: There is a growing demand for reproducible site-specific functionalization of surfaces with biomolecules without introduction of unwanted groups or catalysts, as they may interfere with later applications. The title reactions (see picture) could fulfill these requirements, and four recent applications are discussed.

Fullerenes

N. Martín* ______________ **5431 – 5433**

Fullerene $C_{72}Cl_4$: The Exception that Proves the Rule?

In a stable condition: The first example of a non-IPR hollow fullerene that is more stable than the IPR isomer has been reported for the C_{2v}-C_{72} fullerene (see picture). This molecule has been trapped by the exohedral chlorination reaction that affords the $^{\#11188}C_{72}Cl_4$ molecule, the structure of which has been unambiguously determined by X-ray analyses.

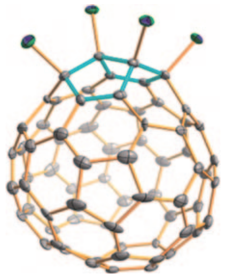

Proteomics

S. Hoogendoorn, L. Willems, B. Florea,
H. Overkleeft* ______________ **5434 – 5436**

Hypersensitive Response to Over-reactive Cysteines

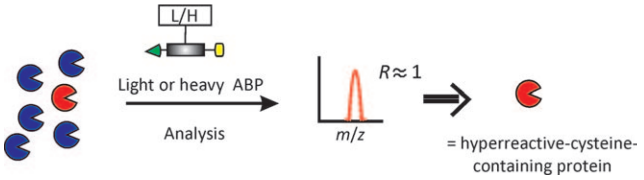

Finding the active cysteine in a hay stack: In the search for active proteins and active-site peptides in a proteome, techniques such as quantitative proteomics and protein profiling with activity-based probes (ABPs; see picture) are commonly used. A recently developed proteomics technique combines these approaches to globally identify reactive cysteines, and possibly other amino acids, in a complex proteome.

For the USA and Canada:
ANGEWANDTE CHEMIE International Edition (ISSN 1433-7851) is published weekly by Wiley-VCH, PO Box 191161, 69451 Weinheim, Germany. Air freight and mailing in the USA by Publications Expediting Inc., 200 Meacham Ave., Elmont, NY 11003. Periodicals postage paid at Jamaica, NY 11431. US POSTMASTER: send address changes to *Angewandte Chemie*, Journal Customer Services, John Wiley & Sons Inc., 350 Main St., Malden, MA 02148-5020. Annual subscription price for institutions: US$ 9442/8583 (valid for print and electronic / print or electronic delivery); for individuals who are personal members of a national chemical society prices are available on request. Postage and handling charges included. All prices are subject to local VAT/sales tax.

Reviews

Green Nanomaterials

D. Klemm,* F. Kramer, S. Moritz, T. Lindström,* M. Ankerfors, D. Gray,* A. Dorris ——— **5438 – 5466**

Nanocelluloses: A New Family of Nature-Based Materials

Cellulose goes nano: Renewed research effort on cellulose has led to nanoscale materials derived from this abundant, renewable, and potentially carbon-neutral source. Microfibrillated cellulose, nanocrystalline cellulose (see polarized microscopy image), and bacterial nanocellulose provide unique product opportunities: gels and foams, structured films of cellulose, and medical implants, respectively.

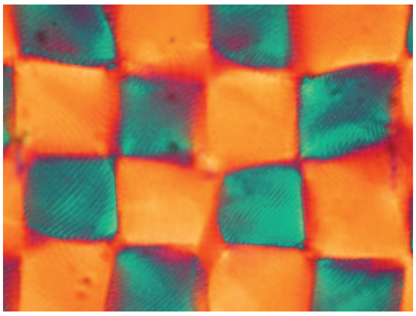

Communications

Heterogeneous Catalysis

B. Genorio, R. Subbaraman, D. Strmcnik, D. Tripkovic, V. R. Stamenkovic, N. M. Markovic* ——— **5468 – 5472**

Tailoring the Selectivity and Stability of Chemically Modified Platinum Nanocatalysts To Design Highly Durable Anodes for PEM Fuel Cells

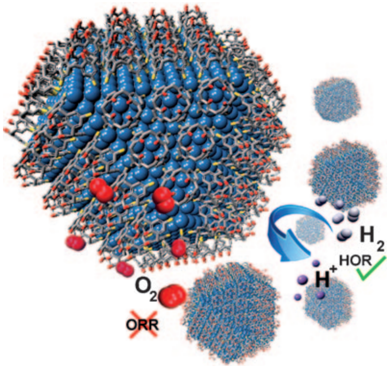

Big and small: Chemically modifying platinum with calix[4]arene yields a highly stable anode catalyst that effectively suppresses the oxidation reduction reaction without altering the maximum activity for the hydrogen oxidation reaction (see picture, Pt blue, C gray, O red, S yellow). This behavior extends from long-range-ordered stepped single-crystal surfaces to nanocatalysts.

Nanostructures

M. Rycenga, X. Xia, C. H. Moran, F. Zhou, D. Qin, Z.-Y. Li, Y. Xia* ——— **5473 – 5477**

Generation of Hot Spots with Silver Nanocubes for Single-Molecule Detection by Surface-Enhanced Raman Scattering

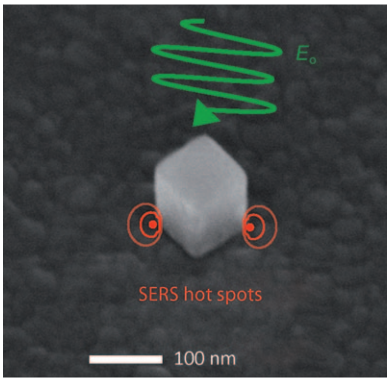

Getting hotter: Hot spots that enable detection of surface-enhanced Raman scattering (SERS) from a single molecule can form at the nanocube–substrate interface by simply depositing a silver nanocube onto a metal substrate (see picture). This new approach offers great simplicity for the formation of robust and fully accessible hot spots, thus providing an effective platform for ultrasensitive detection.

Contents

Cellular Imaging

Y. Kawazoe,* H. Shimogawa, A. Sato, M. Uesugi* **5478 – 5481**

A Mitochondrial Surface-Specific Fluorescent Probe Activated by Bioconversion

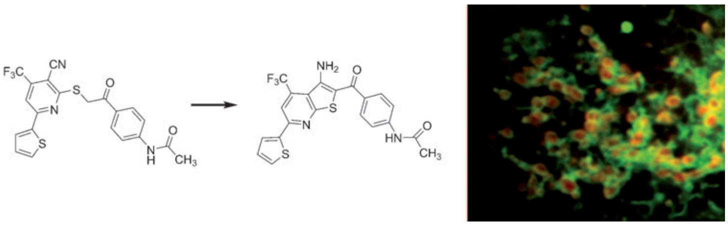

Cell-based image screening of 12000 small molecules with aromatic groups was carried out, and 31 were identified as having potential as fluorescent probes for living cells. One candidate is the first fluorescent probe that specifically stains mitochondrial surfaces. Spectroscopic analyses indicate that the molecule undergoes bioconversion to be fluorescent within cells.

Nanomedicine

C. Zhan, B. Li, L. Hu, X. Wei, L. Feng, W. Fu,* W. Lu* **5482 – 5485**

Micelle-Based Brain-Targeted Drug Delivery Enabled by a Nicotine Acetylcholine Receptor Ligand

Candid candoxin: A 16-residue peptide (CDX) that is derived from candoxin binds with a high affinity to nicotinic acetylcholine receptors (see picture), which are highly expressed on the blood–brain barrier. In vivo biodistribution and the antiglioblastoma effect indicate the potential of CDX as a ligand to enable brain-targeted drug delivery.

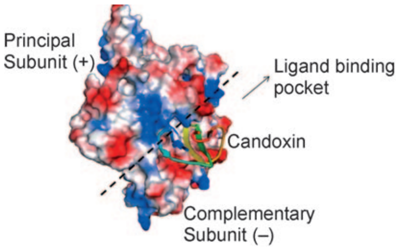

Sensors

X. Chen, L. Li, X. Sun, Y. Liu, B. Luo, C. Wang, Y. Bao, H. Xu, H. Peng* **5486 – 5489**

Magnetochromatic Polydiacetylene by Incorporation of Fe_3O_4 Nanoparticles

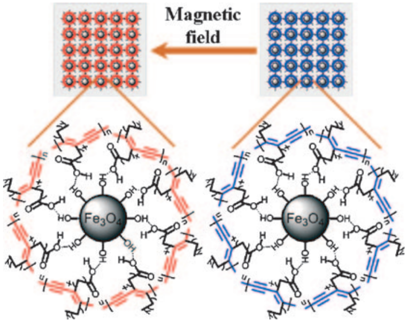

Magnetic personality: Magnetochromatic polydiacetylene has been prepared by the incorporation of superparamagnetic Fe_3O_4 nanoparticles into the polymer network. The composite nanomaterial changes color in a magnetic field through a ready and efficient self-assembly process.

Supramolecular Polymers

A. L. Nussbaumer, D. Studer, V. L. Malinovskii, R. Häner* **5490 – 5494**

Amplification of Chirality by Supramolecular Polymerization of Pyrene Oligomers

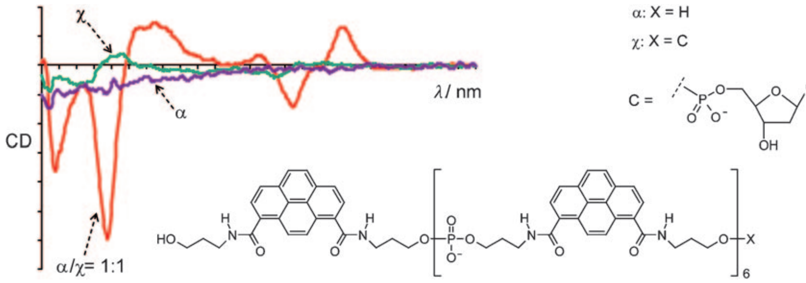

Achiral pyrene oligomers α show remarkable amplification of chirality (see circular dichroism spectra) in the presence of minute quantities of a chiral inductor χ. Spectroscopy and electron microscopy data support a model in which pyrene oligomers form helical, supramolecular polymers by interstrand stacking interactions.

Amyloid Fibrils

J. Adamcik, V. Castelletto, S. Bolisetty,
I. W. Hamley,*
R. Mezzenga* ______ 5495 – 5498

Direct Observation of Time-Resolved Polymorphic States in the Self-Assembly of End-Capped Heptapeptides

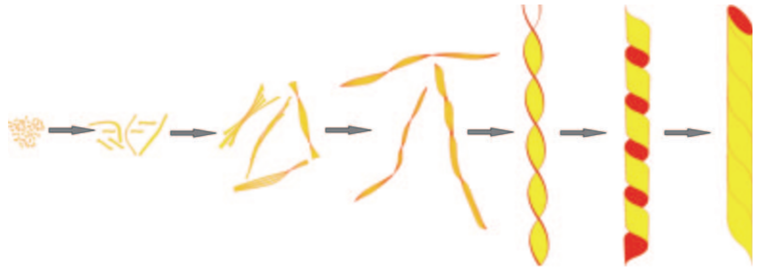

Fibrillation processes in peptides: Structural states in the time-dependent self-assembly of an amyloid heptapeptide were resolved by single-molecule atomic force microscopy. Statistical analysis of the structures and their topological details revealed a continuous evolution of the polymorphs over time from the initial small spherical micelles into protofilaments, helical ribbons, and finally nanotube-like structures (see picture).

Chiral Nanoparticles

A. Guerrero-Martínez, B. Auguié,
J. L. Alonso-Gómez, Z. Džolić,
S. Gómez-Graña, M. Žinić,* M. M. Cid,*
L. M. Liz-Marzán* ______ 5499 – 5503

Intense Optical Activity from Three-Dimensional Chiral Ordering of Plasmonic Nanoantennas

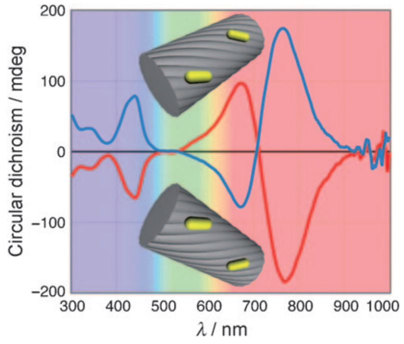

Twisting nanoparticles: Plasmonic circular dichroism was experimentally obtained in chiral 3D organizations of gold nanorods obtained by self-assembly of the nanoantennas onto a fiber template with a twisted morphology. Numerical simulations based on coupled dipoles confirm the crucial role of gold nanorods in this intense circular dichroism.

Heterometallic Complexes

S.-S. Bao, Y. Liao, Y.-H. Su, X. Liang,
F.-C. Hu, Z. Sun, L.-M. Zheng,* S. Wei,*
R. Alberto, Y.-Z. Li, J. Ma* ______ 5504 – 5508

Tuning the Spin State of Cobalt in a Co–La Heterometallic Complex through Controllable Coordination Sphere of La

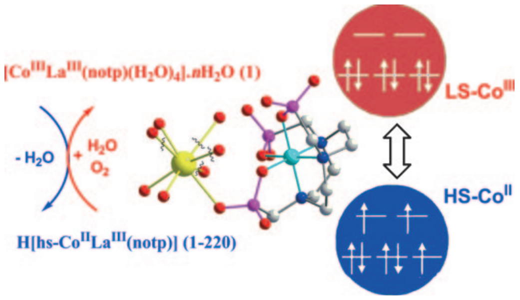

Reversible dehydration of complex **1** switches the spin state of cobalt from low-spin (LS) Co^{III} to high-spin (HS) Co^{II} (see picture) and allows the magnetic moment to be varied from 0.48 μ_B at 120 °C to 4.15 μ_B at 220 °C in fully dehydrated complex **1-220**. $notpH_6$ = 1,4,7-triazacyclononane-1,4,7-triyl-tris(methylenephosphonic acid).

Contents

Imaging Technology

R. Torres Martin de Rosales,* R. Tavaré, R. L. Paul, M. Jauregui-Osoro, A. Protti, A. Glaria, G. Varma, I. Szanda, P. J. Blower* **5509 – 5513**

Synthesis of $^{64}Cu^{II}$–Bis(dithiocarbamate-bisphosphonate) and Its Conjugation with Superparamagnetic Iron Oxide Nanoparticles: In Vivo Evaluation as Dual-Modality PET–MRI Agent

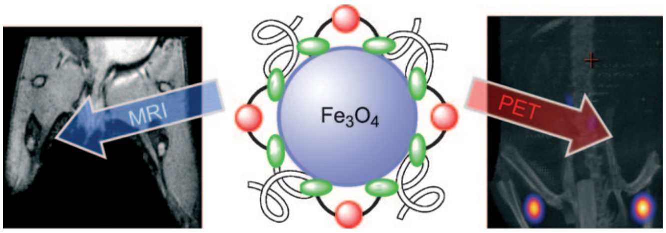

A novel bifunctional chelator combines a dithiocarbamate group for binding the positron-emitter ^{64}Cu (red spheres) for PET imaging and a bisphosphonate group (green ellipsoids) for strong binding to several inorganic materials, such as MRI contrast agents based on superparamagnetic iron oxide nanoparticles and rare-earth metal oxides. The dual PET–MR imaging capabilities of this approach are demonstrated in vivo by imaging lymph nodes using both imaging modalities.

Protein Folding

F. Sziegat, J. Wirmer-Bartoschek, H. Schwalbe* **5514 – 5518**

Characteristics of Human Lysozyme and Its Disease-Related Mutants in their Unfolded States

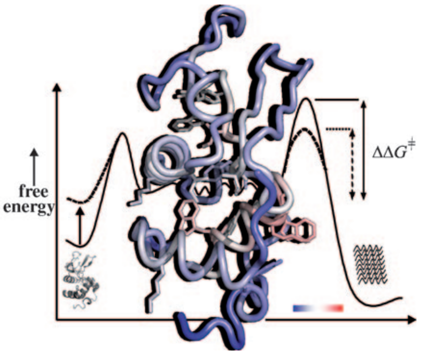

A subtle balance: The residual structure and dynamics in nonnative hen lysozyme, human lysozyme, and in two amyloidogenic mutants have been characterized by NMR spectroscopy at atomic resolution. The degree of residual structure correlates with the ability of the protein to form amyloid fibrils. The free-energy landscape connecting different members of the ensemble of premolten protein states is affected by single-point mutations (see picture).

Organic Electronics

D. H. Wang, D. Y. Kim, K. W. Choi, J. H. Seo, S. H. Im, J. H. Park,* O. O. Park,* A. J. Heeger* **5519 – 5523**

Enhancement of Donor–Acceptor Polymer Bulk Heterojunction Solar Cell Power Conversion Efficiencies by Addition of Au Nanoparticles

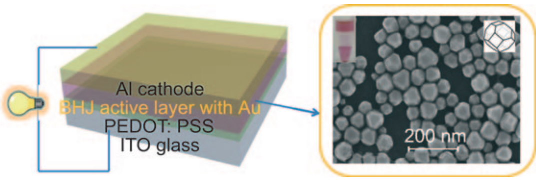

Golden solar cells: Several positive effects arise from the addition of truncated octahedral Au nanoparticles (ca. 70 nm diameter) to bulk heterojunction (BHJ) photovoltaic cells fabricated from a variety of donor polymers and $PC_{70}BM$ as acceptor (see picture). At the optimized blend ratio of Au nanoparticles (5 wt %) in the active layer, the power conversion efficiency increased for all polymer/$PC_{70}BM$ systems under study.

Synthetic Methods

R. B. Bedford,* M. F. Haddow, C. J. Mitchell, R. L. Webster **5524 – 5527**

Mild C–H Halogenation of Anilides and the Isolation of an Unusual Palladium(I)–Palladium(II) Species

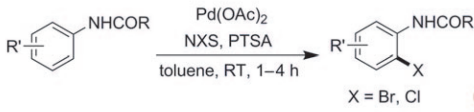

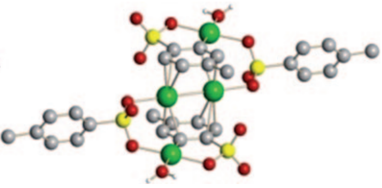

Reducing the load: A facile palladium-catalyzed *ortho*-selective bromination and chlorination of anilides occurs under aerobic conditions at room temperature when *N*-halosuccinimides (NXS) are used in the presence of *p*-toluenesulfonic acid (PTSA). The orthopalladated PTSA complex is not only catalytically competent but also undergoes a reductive process to yield an unusual Pd^{I}–Pd^{II} tetramer (see structure; Pd green, O red, S yellow, C gray).

Catalytic Alkene Dimerization

P. Serna, B. C. Gates* ——— **5528 – 5531**

A Bifunctional Mechanism for Ethene Dimerization: Catalysis by Rhodium Complexes on Zeolite HY in the Absence of Halides

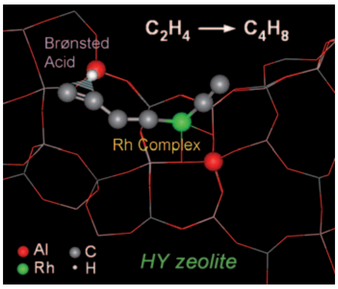

No ligands needed: Rhodium complexes supported on HY zeolite catalyze the formation of C–C bonds by a new mechanism involving cooperation between the metal species and Brønsted acid sites of the zeolite support (see picture). The catalyst operates in the absence of ligands such as halides and shows high selectivity to *n*-butenes, even in an excess of H_2.

Dinuclear Palladium(III) Complexes

J. R. Khusnutdinova, N. P. Rath, L. M. Mirica* ——— **5532 – 5536**

Dinuclear Palladium(III) Complexes with a Single Unsupported Bridging Halide Ligand: Reversible Formation from Mononuclear Palladium(II) or Palladium(IV) Precursors

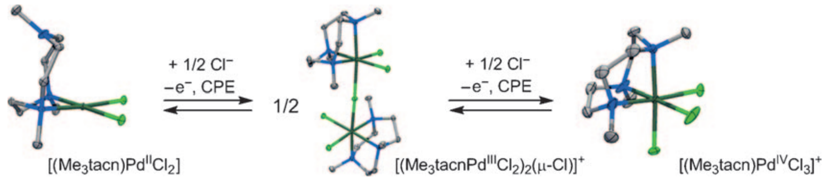

Stable Pd^{III}: Dinuclear Pd^{III} complexes of the tridentate ligand trimethyltriazacyclononane (Me_3tacn) were obtained by one-electron oxidation of mononuclear Pd^{II} precursors. Further oxidation led reversibly to mononuclear Pd^{IV} species. The Pd^{II} and Pd^{III} complexes are shown to be involved in the catalytic Kharasch addition of polyhaloalkanes to alkenes.

Azafullerenes

N. B. Shustova, I. V. Kuvychko, A. A. Popov,* M. von Delius, L. Dunsch, O. P. Anderson, A. Hirsch,* S. H. Strauss,* O. V. Boltalina* ——— **5537 – 5540**

Nitrogen Directs Multiple Radical Additions to the 9,9′-Bi-1-aza(C_{60}-I_h)-[5,6]fullerene: X-ray Structure of 6,9,12,15,18-$C_{59}N(CF_3)_5$

“Dixie cup” packing: Molecules of the first structurally characterized derivative of $(C_{59}N)_2$ bearing trifluoromethyl groups are stacked in register 10.179 Å apart to form a rare non-close-packed arrangement (AAA…; see picture). The presence of the nitrogen atom on the fullerene core results in unique addition patterns in $C_{59}N(CF_3)_{7/9/11}$.

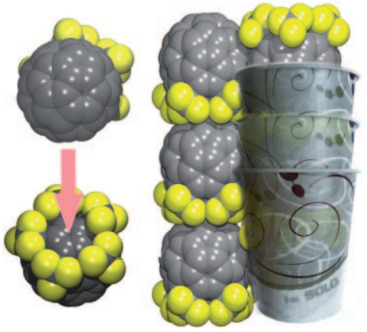

Asymmetric Hydrocyanation

N. Kurono, N. Nii, Y. Sakaguchi, M. Uemura, T. Ohkuma* ——— **5541 – 5544**

Asymmetric Hydrocyanation of α,β-Unsaturated Ketones into β-Cyano Ketones with the [Ru(phgly)$_2$(binap)]/C_6H_5OLi Catalyst System

Enantioselective conjugate addition of HCN to α,β-unsaturated ketones catalyzed by the combined system of [Ru{(*S*)-phgly}$_2${(*S*)-binap}] and C_6H_5OLi has afforded β-cyano ketones in high yield (see scheme). No detectable amount of the corresponding 1,2-adduct was produced and *tert*-$C_4H_9OCH_3$ was the solvent of choice. The cyanation was conducted with a substrate-to-catalyst molar ratio in the range of 200:1–1000:1 at –20–0 °C.

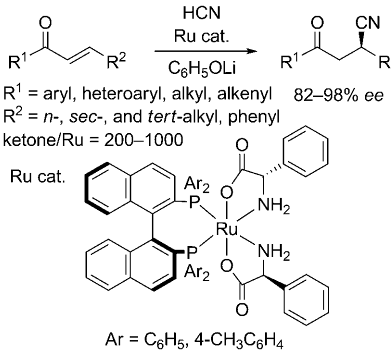

R^1 = aryl, heteroaryl, alkyl, alkenyl
R^2 = *n*-, *sec*-, and *tert*-alkyl, phenyl
ketone/Ru = 200–1000

Ar = C_6H_5, 4-$CH_3C_6H_4$

Contents

C–C Formation

C. C. Lee, Y. Hu,*
M. W. Ribbe* ______________ **5545 – 5547**

Tracing the Hydrogen Source of Hydrocarbons Formed by Vanadium Nitrogenase

Hydrocarbons from CO: The vanadium-nitrogenase-catalyzed reduction of carbon monoxide involves the adenosine triphosphate (ATP)-dependent protonation of CO and the subsequent formation of C–C bonds, leading to the production of small hydrocarbons, such as C_2H_4, C_2H_6, C_3H_6, and C_3H_8 (see picture). Isotope-substitution studies monitored by GC–MS analysis show that protons are the source of hydrogen for the CO reduction.

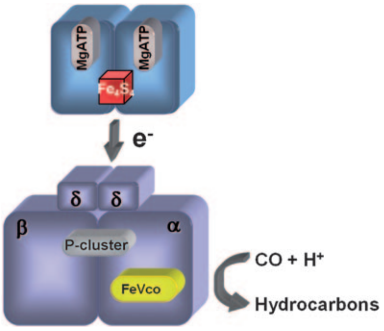

Homogeneous Catalysis

K. Takatsu, R. Shintani,*
T. Hayashi* ______________ **5548 – 5552**

Copper-Catalyzed 1,4-Addition of Organoboronates to Alkylidene Cyanoacetates: Mechanistic Insight and Application to Asymmetric Catalysis

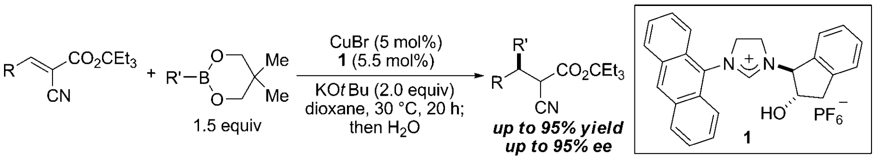

In addition: A copper/N-heterocyclic carbene(NHC)-catalyzed 1,4-addition of organoboronates to alkylidene cyanoacetates was developed, in which the catalytic cycle is proposed to consist of a transmetalation/insertion/ligand exchange. An effective asymmetric variant has also been achieved by the use of a chiral NHC ligand (see scheme).

Dynamic Kinetic Resolution

X. Yang, V. B. Birman* ________ **5553 – 5555**

Nonenzymatic Dynamic Kinetic Resolution of α-(Arylthio)- and α-(Alkylthio)alkanoic Acids

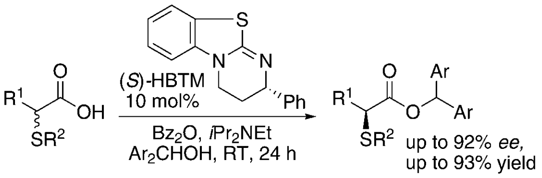

Dynamic solution: The title acids undergo dynamic kinetic resolution during an enantioselective esterification catalyzed by (*S*)-homobenzotetramisole ((*S*)-HBTM; see scheme). This method extends the scope of the carboxylic acid derivatives that are amenable to the nonenzymatic version of this transformation.

Fast NMR Spectroscopy

K. Kazimierczuk,
V. Yu. Orekhov* ______________ **5556 – 5559**

Accelerated NMR Spectroscopy by Using Compressed Sensing

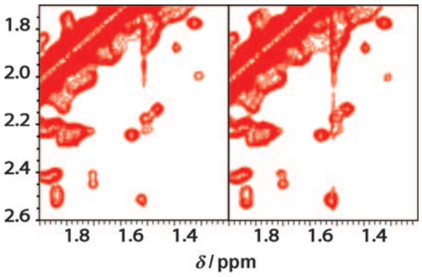

High-quality multidimensional NMR spectra can be obtained from rapidly recorded non-uniformly sampled (NUS) data. The inherent loss of the spectrum quality usually associated with NUS data is compensated by compressed sensing (CS); left spectrum: Nyquist–Shannon sampling, 22 h acquisition time, Fourier transform; right: CS non-linear sampling, 8.5 h acquisition time, l_p norm minimization.

Synthetic Methods

R. Kinjo, B. Donnadieu,
G. Bertrand* ———— 5560 – 5563

Gold-Catalyzed Hydroamination of Alkynes and Allenes with Parent Hydrazine

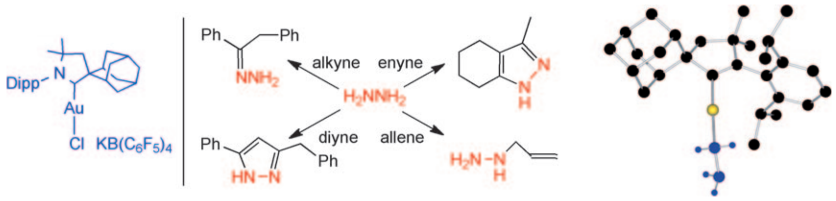

A diverse array of nitrogen-containing compounds were formed by the addition of hydrazine to alkynes, diynes, enynes, and allenes in the presence of cationic gold(I) complexes with a cyclic (alkyl)-(amino)carbene ligand (see scheme; the X-ray crystal structure of the gold–hydrazine complex is shown). This hydroamination is an ideal initial step for the preparation of acyclic and heterocyclic bulk chemicals. Dipp = 2,6-diisopropylphenyl.

Electrochemical Amine Synthesis

J. Kulisch, M. Nieger, F. Stecker, A. Fischer,
S. R. Waldvogel* ———— 5564 – 5567

Efficient and Stereodivergent Electrochemical Synthesis of Optically Pure Menthylamines

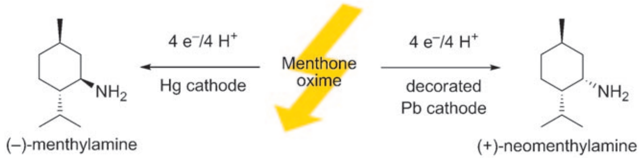

The cathode directs the way to the epimeric menthylamines. The reduction of menthone oxime on a Hg cathode generates (−)-menthylamine as the major product, whereas a Pb cathode gives access to (+)-neomenthylamine (see scheme). In situ decoration of the Pb cathode by small amounts of additives results in clean and quantitative conversions. Furthermore, Pb corrosion is completely prevented in this practical method.

Allylic Etherification

M. Roggen, E. M. Carreira* 5568 – 5571

Enantioselective Allylic Etherification: Selective Coupling of Two Unactivated Alcohols

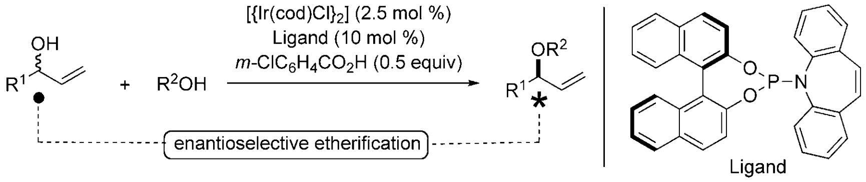

An Ir(P,alkene) complex catalyzes the enantioselective allylic etherification of unactivated secondary allylic alcohols. Useful levels of enantioselectivity and yield were achieved with this operationally easy and robust protocol. Initial kinetic studies indicate a significant rate difference for the substrate enantiomers, allowing for a resolution process. cod = 1,5-cyclooctadiene

Conjugated Macrocycles

J. K. Sprafke, B. Odell, T. D. W. Claridge,
H. L. Anderson* ———— 5572 – 5575

All-or-Nothing Cooperative Self-Assembly of an Annulene Sandwich

Ring-fenced: A 14-component assembly is formed by coordinating 1,4-diazabicyclo-[2.2.2]octane (DABCO) to a [12]porphyrin nanoring. The 24 zinc–nitrogen interactions in this sandwich complex lock each conjugated macrocycle into a planar conformation, dramatically sharpening the near-IR absorption band. This result highlights the scope of double-strand formation as a way of creating nano-objects with well-defined shapes.

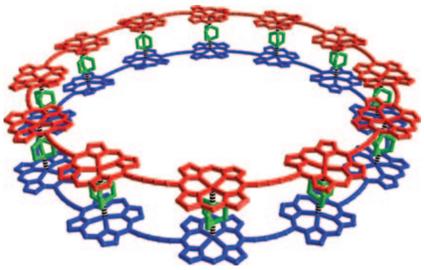

Contents

Gas-Phase Structures

A hint of cassis: By a combination of microwave spectroscopy and quantum chemistry, the gas-phase structures of the Cassyrane stereoisomers and its dihydro derivatives have been determined, and correlated with their olfactory properties. Superposition analyses of the structures (see picture; black Cassyrane, silver Oxane, red O, yellow S) reveal the importance of the 5*S* configuration on the cassis odor, with the 2*S*,5*R* isomers being the most intense.

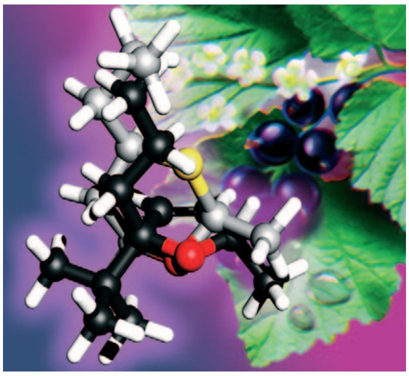

Fluorescence Nanoscopy

Clearing the haze: Stimulated emission depletion (STED) nanoscopy on single DNA strands reveals details with an up to five- to sixfold improved resolution over confocal microscopy (see images). Thus STED nanoscopy allows features to be distinguished down to the persistence length of DNA (ca. 50 nm) without promoting any significant additional photodamage, such as photobleaching or photonicking.

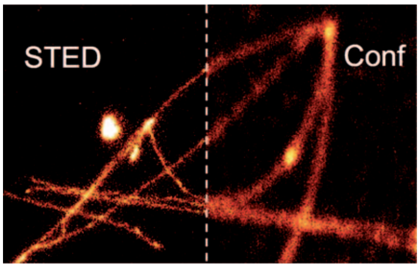

Supporting information is available on www.angewandte.org (see article for access details).

A video clip is available as Supporting Information on www.angewandte.org (see article for access details).

This article is available online free of charge (Open Access).

Service